JGR Oceans

RESEARCH ARTICLE
10.1029/2020JC017040

Key Points:

- The volume of Subantarctic Mode Water (SAMW) in the Southern Ocean has increased by ~11% since the 1950s
- The SAMW volumes in the upper and lower layers vary out of phase with each other on decadal time scales in the Indian and Pacific sectors
- The decadal changes in the SAMW volume in the Indian and Pacific sectors appear to compensate each other

Correspondence to:
Y. Luo,
yiyongluo@ouc.edu.cn

Citation:
Jing, W., & Luo, Y. (2021). Volume budget of Subantarctic Mode Water in the Southern Ocean from an ocean general circulation model. *Journal of Geophysical Research: Oceans*, *126*, e2020JC017040. https://doi.org/10.1029/2020JC017040

Received 1 FEB 2021
Accepted 3 OCT 2021

Volume Budget of Subantarctic Mode Water in the Southern Ocean From an Ocean General Circulation Model

Wandi Jing[1] and Yiyong Luo[1,2]

[1]Frontier Science Center for Deep Ocean Multispheres and Earth System (FDOMES) and Physical Oceanography Laboratory, Ocean University of China, Qingdao, China, [2]Laboratory for Ocean Dynamics and Climate, Qingdao Pilot National Laboratory for Marine Science and Technology, Qingdao, China

Abstract The volume budget of Subantarctic Mode Water (SAMW) in the Southern Ocean (SO) is examined using a 0.1° ocean model output from 1950 to 2017. The results show that air–sea buoyancy fluxes, advective exports, and diapycnal mixing are all important to the SAMW volume budget. A climatological mean analysis finds that, for the SO as a whole, water in the SAMW density range (σ_θ = 26.5 – 27.1 kg m^{-3}) is balanced between the following: formation due to air–sea buoyancy fluxes (19.6 ± 2.7 Sv), removal due to advective export northward out of the SO (14.2 ± 0.9 Sv), destruction due to diapycnal mixing (3.1 ± 2.2 Sv), and storage (2.3 ± 2.6 Sv). Decadal changes in the SAMW volume in the Indian and Pacific sectors display a two-layer density structure, in which the volumes of the upper and lower layers vary predominantly out of phase with each other. In addition, the SAMW volume changes in the Indian and Pacific sectors appear to compensate each other on decadal time scales. The volume of SAMW in the SO has increased by ~11% since the 1950s, and this increase tends to emerge gradually from denser to lighter layers. The increased SAMW volume mainly results from a consistent increase in oceanic buoyancy gain over the outcropping area at approximately 27.1 kg m^{-3}.

Plain Language Summary Subantarctic Mode Water in the Southern Ocean (SO) is a distinct water mass with a thickness of several hundred meters, and its formation and export play an important role in distributing heat and carbon on a global scale. Our study employs a fine-resolution ocean model and examines changes in this important water mass from 1950 to 2017. We find that its volume has significantly increased since the 1950s, which has been caused by a consistent increase in buoyancy gain by the ocean over its formation area. Moreover, this mode water experiences opposing volume changes with similar amplitudes in the upper and lower layers on decadal time scales, that is, the upper layer gains (or loses) volume while the lower layer loses (or gains) volume. These findings improve our understanding of heat content and carbon uptake in the SO.

1. Introduction

Subantarctic Mode Water (SAMW) is a distinct water mass that occurs north of the Subantarctic Front (SAF) in the Southern Ocean (SO), and it contains low potential vorticity (PV) waters in the thick winter mixed layer as well as in those being subducted into the thermocline (McCartney, 1977). The physical properties of SAMW vary significantly along its circumpolar path; it has a potential density range from 26.5 to 27.1 kg m^{-3} (Hanawa & Talley, 2001). The formation and export of SAMW supply the upper cell of the meridional overturning circulation and play an important role in global heat, freshwater, carbon, and nutrient budgets (Gao et al., 2017; Sabine et al., 2004; Sloyan & Rintoul, 2001).

Extensive studies have been performed to understand the formation of and property changes in SAMW. For example, McCartney (1982) attributed the formation of and change in SAMW to air–sea buoyancy fluxes. By analyzing two mooring observations in the southeast Indian Ocean and southeast Pacific Ocean, Tamsitt et al. (2020) also showed that wintertime surface ocean heat loss plays an important role in SAMW formation. Rintoul and England (2002) found that Ekman transport has a significant effect on the formation of and change in SAMW. Sallée et al. (2008) showed that eddy heat diffusion contributes significantly to the SAMW property variability. Sallée et al. (2010) pointed out that Ekman pumping, geostrophic mean flow, and eddy-induced advection all contribute to the subduction of SAMW. Using a gridded Argo product for

the years 2004–2018, Li et al. (2021) separately considered SAMW formation processes within the mixed layer and below the mixed layer, and found that SAMW in the mixed layer is mainly formed by air-sea buoyancy fluxes and SAMW in the interior is mainly formed by instantaneous subduction rate.

Regarding the temporal variation in SAMW, Naveira Garabato et al. (2009) analyzed 24 transects of measurements across the Drake Passage and found that the interannual variability in SAMW is mainly driven by the change in wintertime air–sea turbulent heat fluxes and net evaporation, which is in turn modulated by the El Niño-Southern Oscillation (ENSO). Kwon (2013) discussed the time-dependent formation and subduction of SAMW in an eddy-permitting coupled climate model and found that the interannual variability in the subduction rate of SAMW is partly controlled by the change in the wintertime mixed layer depth (MLD). More recently, Cerovečki et al. (2019) and Lu et al. (2020) found that advective processes are also important for the interannual variability in the SAMW properties and thickness. By analyzing Argo data and mooring observations, recent studies also found that the interannual variability in SAMW appears to have large-scale dipole structures in both the Indian and Pacific sectors. For example, Meijers et al. (2019) discussed the spatial and temporal variability in the Pacific SAMW and found that the thicknesses of SAMW in the central and eastern Pacific Ocean vary predominantly out of phase with each other, which is controlled by the wind stress and turbulent heat fluxes related to the Southern Annular Mode (SAM) and ENSO. Tamsitt et al. (2020) showed that the out-of-phase variability in the Pacific sector is also evident in the Indian sector. Cerovečki and Meijers (2021) demonstrated that these dipoles are strongly correlated with the interannual variability in wintertime mean sea level pressure anomalies.

Argo observations have also shown significant changes in SAMW on a longer time scale. For example, Gao et al. (2017) found that the SAMW volume increased from 2005 to 2015, which was mainly caused by the change in wind forcing. Qu et al. (2020) identified that the subduction rate of SAMW increased during 2005–2019, which was associated with the change in the wind stress curl over the SAMW formation region. In contrast, Hong et al. (2020) showed that the SAMW volume in the Indian sector decreased by 10% from 2004 to 2018. As noted in Hong et al. (2020), the main reason why they and Gao et al. (2017) reached an opposite conclusion is the SAMW definition employed, that is, SAMW was defined using a narrower density range with imposing a low-PV constraint in their study. With a similar definition of SAMW as Hong et al. (2020), Xu et al. (2021) found that SAMW in the whole SO became warmer, fresher, lighter, and weaker during 2004–2019. Although Xu et al. (2021) showed that these property changes in SAMW also existed before the Argo era through an analysis of a long ocean general circulation model (OGCM) simulation during 1955–2017, they did not examine the SAMW volume change during that time period specifically.

Recently, studies have evaluated the volume budget of SAMW. In particular, Cerovečki et al. (2013) analyzed the data-assimilating, eddy-permitting Southern Ocean State Estimate (SOSE) for 2005–2006 and concluded that SAMW is formed by air–sea buoyancy fluxes, destroyed by diapycnal mixing, and exported northward out of the SO. Furthermore, Cerovečki and Mazloff (2016) used the data-assimilating results for 2008–2010 to obtain a three-dimensional and time-varying volume budget for individual isopycnal layers and confirmed that air–sea buoyancy fluxes, diapycnal mixing, and advection are all important to the SAMW volume budget. They also found that the formation and destruction of SAMW occur over a large latitude range because of the seasonal migration of the outcrop window, and the strongest formation is due to wintertime surface ocean heat loss occurring equatorward of the SAF. However, their study notes that how these processes vary interannually and within a changing climate need to be addressed in future works. By analyzing the Argo data and the Estimating the Circulation and Climate of the Ocean version 4 (ECCO4) reanalysis, a recent study by Portela et al. (2020) used a density–spice framework to investigate the main mechanisms driving the volume change in interior water masses in the Southern Hemisphere oceans through a volume budget analysis between 2006 and 2015. They found that SAMW exhibits a two-layer density structure with the same spiciness but opposite trend signs, i.e., the upper layer gains volume through subduction and diapycnal transformation, and the lower layer loses volume by means of isopycnal and diapycnal transformation. In addition, they showed that both subduction and interior mixing are important to explain the SAMW volume trends. In their study, however, only the interior SAMW was discussed, and SAMW within the deep mixed layer was not taken into consideration.

As reviewed above, SAMW variability has been extensively studied during the Argo era in previous studies. However, limited by sparse data, SAMW variability on decadal and longer time scales is not yet well

documented. In this study, we examine the volume budget of SAMW by using an eddy-revolving ocean model output ranging from 1950 to 2017. In particular, our study focuses on the decadal variability and long-term changes in the SAMW volume. As is shown later, our new findings are as follows: (a) the volume of SAMW in the SO has increased by ~11% since the 1950s, (b) the SAMW volumes in the upper and lower layers vary predominantly out of phase with each other on decadal time scales in the Indian and Pacific sectors, and (c) the decadal changes in the SAMW volume in the Indian and Pacific sectors appear to compensate each other.

The rest of this paper is organized as follows. Section 2 introduces the data and methods and compares the model output with available observations. Section 3 describes the climatological mean and annual cycle of the SAMW volume. Section 4 presents the interannual variability in the SAMW volume. Section 5 discusses the decadal variability and long-term change in the SAMW volume. Section 6 concludes the paper with a summary and discussion.

2. Data and Methods

2.1. Model Output

The present study primarily uses the hindcast simulation of OGCM for the Earth Simulator (OFES), which is based on the Geophysical Fluid Dynamics Laboratory's Modular Ocean Model. The horizontal resolution of OFES is 0.1° in both latitude and longitude, and it has 54 vertical levels with varying layer thicknesses, from 5 m at the surface to 330 m at the maximum depth of 6,065 m. The model is spun up for 50 years with monthly climatological atmospheric forcings from the National Centers for Environmental Prediction (NCEP)/National Center for Atmospheric Research (NCAR) reanalysis and then forced by daily mean NCEP/NCAR reanalysis data from 1950 to 2017 (e.g., Aoki et al., 2007, 2015). More details on the model and simulation can be found in Sasaki et al. (2008). For this study, we use the monthly mean model output from 1950 to 2017, which is obtained from the Asia Pacific Data Research Center (http://apdrc.soest.hawaii.edu/dods/public_ofes/OfES/ncep_0.1_global_mmean).

The OFES simulation has been shown to be reliable for both basin-scale and mesoscale dynamic studies of the SO, and it captures the intraseasonal to decadal variability well compared with the observations (e.g., Sasaki et al., 2008). For example, the model is successful in reproducing the structure of the deep mixed layer in the SO, which is crucial for SAMW formation (Aoki et al., 2007). OFES captures the frontal structures and the trends of temperature around the Antarctic Circumpolar Current (ACC) (Aoki et al., 2015). Although ACC transport through the Drake Passage in OFES (141.7 Sv) is slightly larger than the observations (134.0 Sv), its weak positive trend during the past decades is consistent with observations (Sasaki et al., 2008).

2.2. Walin Analysis

By combining heat and volume budgets for an isothermal layer, Walin (1982) developed a method to estimate the water mass transformation due to surface air–sea fluxes and diffusive fluxes within the ocean interior (Downes et al., 2011). This method has been extended to density coordinates (e.g., Marshall et al., 1999; Nurser et al., 1999) and is widely used in the SO (Cerovečki et al., 2013; Cerovečki & Mazloff, 2016; Iudicone, Madec, Blanke, & Speich, 2008; Sloyan & Rintoul, 2001). In more detail, the water mass formation rate (FR) in the density layer σ, defined as $\sigma - \Delta\sigma/2 < \sigma < \sigma + \Delta\sigma/2$, can be deduced from the difference in the transformation rates (TR):

$$\mathrm{FR}(\sigma,t) = \mathrm{TR}(\sigma - \Delta\sigma/2,t) - \mathrm{TR}(\sigma + \Delta\sigma/2,t) \tag{1}$$

The water mass transformation rate is given by:

$$\mathrm{TR}(\sigma,t) = \mathrm{F}(\sigma,t) - \frac{\partial \mathrm{D}(\sigma,t)}{\partial\sigma} \tag{2}$$

where D represents the diffusive density flux across the isopycnal surface σ in the interior ocean (Nishikawa et al., 2013), and $\mathrm{F}(\sigma,t)$ and $-\partial \mathrm{D}(\sigma,t)/\partial\sigma$ represent the transformation rate due to air–sea buoyancy fluxes

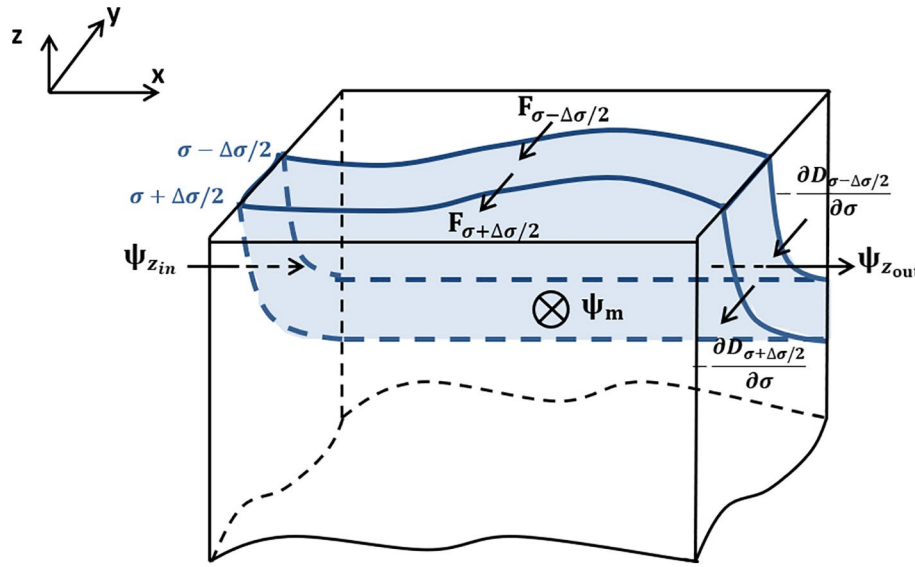

Figure 1. Schematic of the control volume V bounded by the surface outcropping area, the two isopycnal surfaces $\sigma - \Delta\sigma/2$ and $\sigma + \Delta\sigma/2$, the eastern and western boundaries, and the northern boundary (30°S). $F_{\sigma-\Delta\sigma/2}$ and $F_{\sigma+\Delta\sigma/2}$ represent the transformation rate due to air–sea buoyancy fluxes across $\sigma - \Delta\sigma/2$ and $\sigma + \Delta\sigma/2$, respectively; $-\partial D_{\sigma-\Delta\sigma/2}/\partial\sigma$ and $-\partial D_{\sigma+\Delta\sigma/2}/\partial\sigma$ are the transformation rates due to diapycnal mixing across $\sigma - \Delta\sigma/2$ and $\sigma + \Delta\sigma/2$, respectively; $\psi_{z_{in}}$ and $\psi_{z_{out}}$ represent zonal transport into and out of the region, respectively; and ψ_m is the meridional transport across 30°S. This schematic is modified from Figure 1 of Cerovečki and Mazloff (2016).

and interior diapycnal mixing, respectively. A positive TR represents a transformation toward denser water in response to ocean cooling or evaporation.

Furthermore, the transformation rate due to air–sea buoyancy fluxes can be expressed as:

$$F(\sigma,t) = \frac{1}{\Delta\sigma}\iint_{A_\sigma} B(\sigma,t)\,dA \tag{3}$$

where A_σ is the outcropping area within the density range $\sigma - \Delta\sigma/2 < \sigma < \sigma + \Delta\sigma/2$, and $\Delta\sigma$ is chosen to be 0.1 kg m^{-3} in this study; dA is a surface element of A_σ; and $B(\sigma,t)$ is the air–sea buoyancy flux, which can be further written as:

$$B(\sigma,t) = -\frac{\alpha Q_{net}}{C_p} + \beta\rho_0 S_0 (E - P) \tag{4}$$

where α and β are the thermal expansion and saline contraction coefficients, respectively; ρ_0 and S_0 represent sea surface density and salinity, respectively; E and P are evaporation and precipitation, respectively; C_p is the heat capacity of sea water; and Q_{net} is the net air–sea heat flux (which is positive for ocean heat gain). The terms on the right-hand side of Equation 4 represent the contributions from the heat flux and freshwater flux, respectively.

2.3. Volume Budget Analysis

Following previous studies (Cerovečki et al., 2013; Cerovečki & Mazloff, 2016), the volume budget analysis considers a control volume bounded by the surface outcropping area, the two isopycnal surfaces $\sigma - \Delta\sigma/2$ and $\sigma + \Delta\sigma/2$, the eastern and western boundaries, and the northern boundary at 30°S (Figure 1). Based on volume conservation, the temporal variation in the volume between the two isopycnal surfaces $\sigma - \Delta\sigma/2$ and $\sigma + \Delta\sigma/2$ is balanced by the formation rate due to air–sea buoyancy fluxes, advective transport into or out of the region, and diapycnal mixing in the interior ocean expressed as:

$$\frac{\partial V}{\partial t} = F_{\sigma-\Delta\sigma/2} - F_{\sigma+\Delta\sigma/2} + \left(-\frac{\partial D_{\sigma-\Delta\sigma/2}}{\partial\sigma} + \frac{\partial D_{\sigma+\Delta\sigma/2}}{\partial\sigma}\right) + \psi_{z_{in}} - \psi_{z_{out}} + \psi_m \tag{5}$$

where $\partial V/\partial t$ is the rate of the volume change or the storage rate, $F_{\sigma-\Delta\sigma/2} - F_{\sigma+\Delta\sigma/2}$ is the formation rate due to air-sea buoyancy fluxes (air-sea formation), $\psi_{z_{in}} - \psi_{z_{out}}$ is the net zonal transport, ψ_m is the meridional transport, and $-\left(\partial D_{\sigma-\Delta\sigma/2}/\partial\sigma\right) + \left(\partial D_{\sigma+\Delta\sigma/2}/\partial\sigma\right)$ represents the contribution from diapycnal mixing, which denotes the net effect of all mixing processes and is estimated here as a residual of the other terms in Equation 5 (e.g., Cerovečki et al., 2013; Downes et al., 2011; Marsh et al., 2000).

In this study, SAMW is defined as all waters in the potential density range of $\sigma_\theta = 26.5 - 27.1\,\mathrm{kg\,m^{-3}}$ without imposing a low-PV constraint. This definition of SAMW is common in SAMW thickness and volume studies (e.g., Cerovečki et al., 2013; Gao et al., 2017). Walin analysis is used to estimate the water mass transformation. Note that although the Walin analysis provides a natural isopycnal framework for the water mass analysis, it does not account for the role of PV fluxes and thus is not the most suitable tool to analyze the volume budget of a low-PV pool (Cerovečki & Giglio, 2016). A formalism that relates the volume budget to the PV budget was developed to study the subtropical mode water in the North Atlantic by Deremble and Dewar (2013), which provides a better version of the mode water volume budget analysis.

The results of the volume budget shown below are obtained based upon the monthly output of OFES during 1950–2017. Specifically, the volume (V) of an isopycnal layer is calculated by dx× dy × dh, in which dx and dy are the spacing of the model grid, and dh is the thickness of the layer with its upper and lower surfaces being $\sigma - \Delta\sigma/2$ and $\sigma + \Delta\sigma/2$, respectively. The air-sea transformation rate across σ is estimated by integrating the air-sea buoyancy fluxes over the outcropping area between $\sigma - \Delta\sigma/2$ and $\sigma + \Delta\sigma/2$. The zonal and meridional transports are calculated by u× dy × dh and v× dx × dh, in which u and v are the zonal and meridional velocities, respectively.

In the following analysis, the SO is separated into the Atlantic Ocean (AO), Indian Ocean (IO), and Pacific Ocean (PO) sectors. Specifically, the meridional boundaries of these sectors are 20°E, 150°E, and 290°E. The northern boundary is 30°S and the southern boundary is the 27.1 kg m^{-3} isopycnal, which varies with time in this analysis.

2.4. Model Output Validation

To further validate the OFES output, the observed monthly gridded fields of temperature and salinity made by Roemmich and Gilson (2009) are obtained from the Argo website (http://sio-argo.ucsd.edu/RG_Climatology.html). These data cover the period of 2004–2017 and have a horizontal resolution of 1° × 1° and 58 vertical levels from the surface to a depth of 2,000 m.

Since the deep winter mixed layer plays an important role in the formation of SAMW (Dong et al., 2008; Hanawa & Talley, 2001; McCartney, 1977), we first compare the climatological winter MLD between the model and observation data (black contours in Figures 2a and 2b). Here, the MLD is defined as the depth at which the water density is 0.03 kg m^{-3} denser than that at the sea surface. In both OFES and Argo, the deep mixed layer appears to the north of the SAF, and its depth is shallow in the Atlantic and western Indian sectors but deep in the Pacific and eastern Indian sectors. A comparison of the climatological mean SAMW thickness between the model and observation data is also shown in Figures 2a and 2b. While the modeled SAMW thickness appears to be slightly thicker, its distribution is quite similar to that in the observations, that is, in OFES and Argo, the SAMW thickness is relatively thin (~600 m) in the Atlantic and western Indian sectors but reaches 1,000–1,200 m in the Pacific and eastern Indian sectors. These above features of the MLD and SAMW are in agreement with previous studies (Gao et al., 2017; McCartney, 1982; Meijers et al., 2019), that is, the deep MLD and SAMW thickness are not evenly distributed around the SO but mainly occur in large "pools."

Figures 2c and 2d show a comparison of the interannual variability in the deep winter MLD and annual mean SAMW volume between OFES and Argo. While the MLD and SAMW volume appears to be larger in OFES than in Argo, it is clear that the model captures the interannual variability in both the MLD and SAMW volume quite well. In particular, there is an increasing trend from 2004 to 2017 in OFES and Argo, which is consistent with that of Gao et al. (2017).

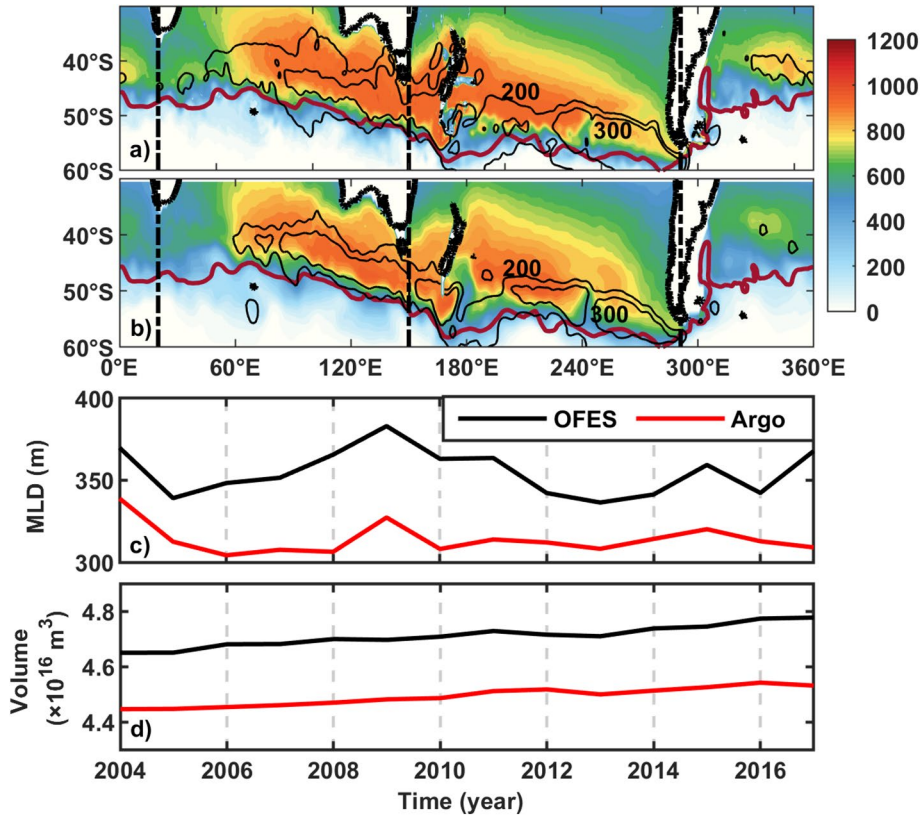

Figure 2. Distribution of climatological mean Subantarctic Mode Water (SAMW) thickness (color; m) and the September mixed layer depth (MLD) (black contours; m) in (a) ocean general circulation model for the Earth Simulator (OFES) and (b) Argo. The climatology is obtained by averaging over the period of 2004–2017. The red curve represents the Subantarctic Front given by Orsi et al. (1995). The black dashed-dotted lines are the boundaries between the ocean sectors. Interannual variability in (c) the deep September MLD (>200 m) and (d) the annual mean SAMW volume from 2004 to 2017 in OFES (black lines) and Argo (red lines).

Figure 3 compares the modeled SAMW thickness in individual isopycnal layers with the observations. In OFES and Argo, the SAMW density gradually increases from the south Indian Ocean to the southeast Pacific Ocean. In the Indian sector, SAMW is mainly located to the south of Australia at the approximately 26.8 kg m^{-3} isopycnal layer, and its thickness reaches 400 m. In the Pacific sector, SAMW occupies the central and eastern basins at the approximately 26.9 and 27.0 kg m^{-3} isopycnal layers, respectively. In the Atlantic sector, although SAMW appears to be much thinner compared to those in the Indian and Pacific sectors, there are still two regions that are recognizable by relatively thick mode water: one is located to the north of the SAF at approximately 27.1 kg m^{-3} and the other is located further north at approximately 26.5 kg m^{-3}.

Therefore, in addition to the realism of the model characteristics as described in previous studies (Aoki et al., 2007, 2015 ; Sasaki et al., 2008), the favorable model-observation comparisons discussed above provide us further confidence that this OFES output is reliable for studying the volume budget of SAMW and its climate variability.

3. Climatological Mean and Annual Cycle

3.1. Climatological Mean

Table 1 lists the climatological mean SAMW volumes in each ocean sector, which are obtained by averaging over the period of 1950–2017 in OFES. The PO occupies approximately 49% of the total SAMW, with the rest being contributed by the IO (36%) and AO (15%). The relatively small contribution from the AO is because the SAMW appears to be thin and have a small spatial extent (Figure 2a).

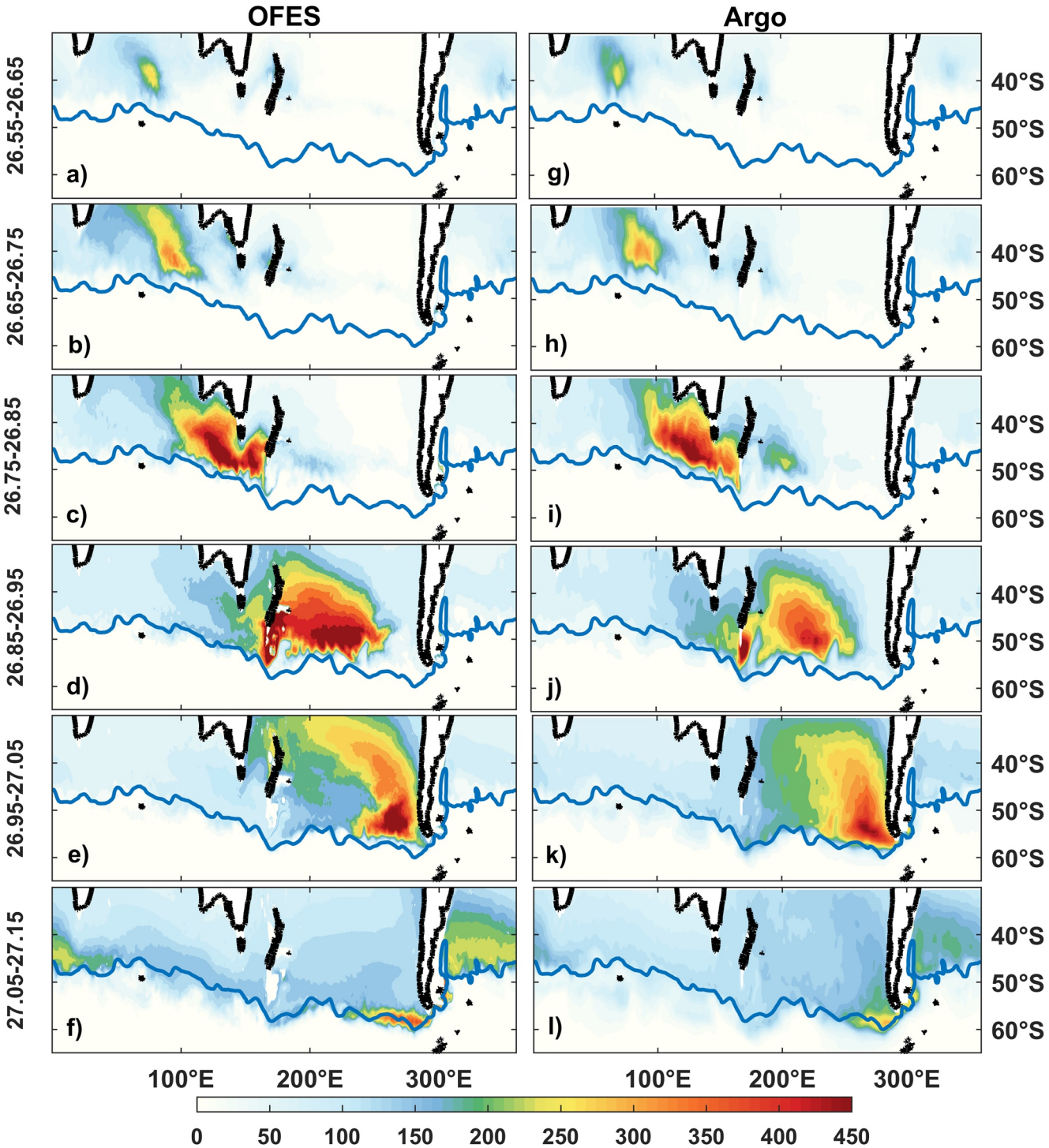

Figure 3. Distribution of climatological mean Subantarctic Mode Water thickness (color; m) in different isopycnal layers in ocean general circulation model for the Earth (left) and Argo (right). The climatological mean is obtained by averaging over the period of 2004–2017. The density range of individual isopycnal layers is indicated to the left of the panel. The blue curve represents the Subantarctic Front given by Orsi et al. (1995).

According to Equation 5, the storage rate of the SAMW volume is balanced by the formation rate due to air–sea buoyancy fluxes, transport into or out of the region, and diapycnal mixing in the interior ocean. To examine the relative contribution of each process to the volume storage rate, all the terms, including the storage rate, in the SAMW volume budget Equation 5 are calculated by using the monthly model output,

Table 1
Volumes of Subantarctic Mode Water in Different Ocean Sectors

Ocean sector	Longitude range	Total volume ($\times 10^{16}$ m^3)
Indian Ocean (IO)	20°E – 150°E	1.6 ± 0.05
Pacific Ocean (PO)	150°E – 290°E	2.2 ± 0.04
Atlantic Ocean (AO)	290°E – 20°E	0.7 ± 0.06
Southern Ocean (SO)	0°E – 360°E	4.5 ± 0.15

and then an annual mean is obtained by averaging the 12 months within that year and the climatological mean by further averaging over the 68 years of the model simulation. First, it is clear that the storage rate of the climatological mean SAMW volume appears to be close to zero for each individual ocean sector (Figure 4). This result is in contrast to those from previous studies, in which a relatively short data record is used for analysis (e.g., Cerovečki et al., 2013; Cerovečki & Mazloff, 2016; Portela et al., 2020).

In the IO (green bars in Figure 4), SAMW is predominantly formed by air–sea buoyancy fluxes (18.5 ± 2.2 Sv). The formation by air–sea buoyancy fluxes is largest in the IO compared to that in the other ocean sectors, which is consistent with the finding of Marsh et al. (2000). This volume is removed by net zonal advection (12.0 ± 1.1 Sv), meridional transport across 30°S (3.1 ± 0.5 Sv), and diapycnal mixing (2.6 ± 1.8 Sv). By using the SOSE data for 2008–2010, Cerovečki and Mazloff (2016) estimated the SAMW volume budget in the density range of 26.7–27.1 kg m^{-3} and found that the largest SAMW formation is in the IO, which is in agreement with our result. Sloyan and Rintoul (2001) used a box inverse model with hydrographic data covering 1976–1994 and examined the mean volume budget of water in a broader density range of 26.0–27.0 kg m^{-3}. They found that in the IO, the formation by air–sea buoyancy fluxes is 16.1 ± 3Sv and the destruction by diapycnal mixing is 4 ± 2 Sv. If our estimation was confined by the same density range as that of Sloyan and Rintoul (2001), the formation by air–sea buoyancy fluxes would be 17.4 ± 2.2 Sv, and the destruction by diapycnal mixing would be 3.3 ± 1.7 Sv.

An investigation of individual isopycnal layers (Figure 5a) finds that the formation (destruction) of SAMW in the IO by air–sea buoyancy fluxes (diapycnal mixing) occurs primarily at 26.8 and 26.9 kg m^{-3}. The net zonal transport acts to export the SAMW for all the isopycnals and appears to be stronger in denser layers. The above results are qualitatively consistent with those of Cerovečki et al. (2013). In addition, the formation (destruction) of diapycnal mixing tends to compensate for the destruction (formation) by air–sea buoyancy fluxes (Figure 5a). These results are consistent with those of Iudicone, Madec, Blanke, and Speich (2008), who found that the transformation due to surface fluxes in the same density range is almost compensated by diapycnal mixing in the SO.

In the PO (red bars in Figure 4), all SAMW is supplied by zonal transport (11.7 ± 1.2 Sv), most of which is destroyed by air–sea buoyancy fluxes (7.9 ± 1.7 Sv), and the rest is exported northward out of the SO by meridional transport (3.8 ± 0.5 Sv). By using hydrographic data, Hartin et al. (2011) estimated the interocean transport of SAMW in the density range of 26.8–27.0 kg m^{-3} from the PO to the AO to be 4.4 ± 0.6 Sv. If our estimation was confined by the same density range as that of Hartin et al. (2011), the transport would be 6.6 ± 1.5 Sv, which is comparable to the result from Hartin et al. (2011). A negative contribution to SAMW

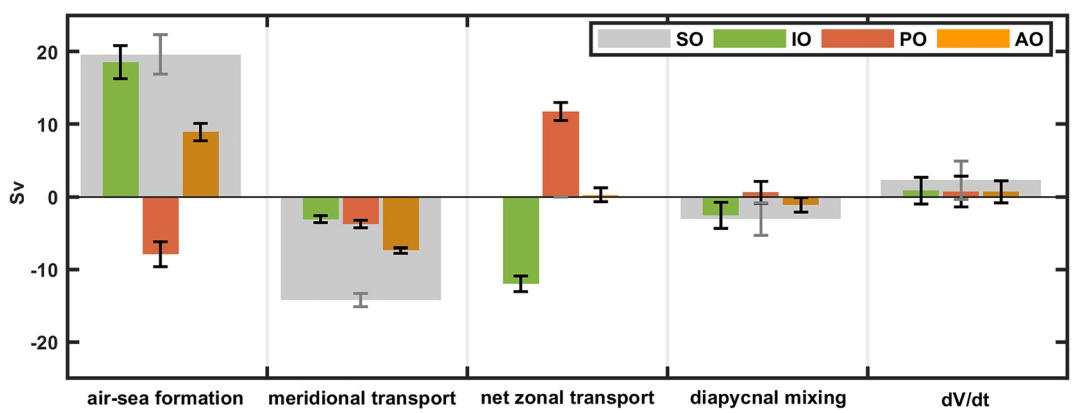

Figure 4. Climatological mean Subantarctic Mode Water (SAMW) volume budget terms in the SAMW density range of 26.5–27.1 kg m^{-3}, which is obtained by averaging over the period of 1950–2017. The error bars denote the standard deviations of annual mean values during 1950–2017.

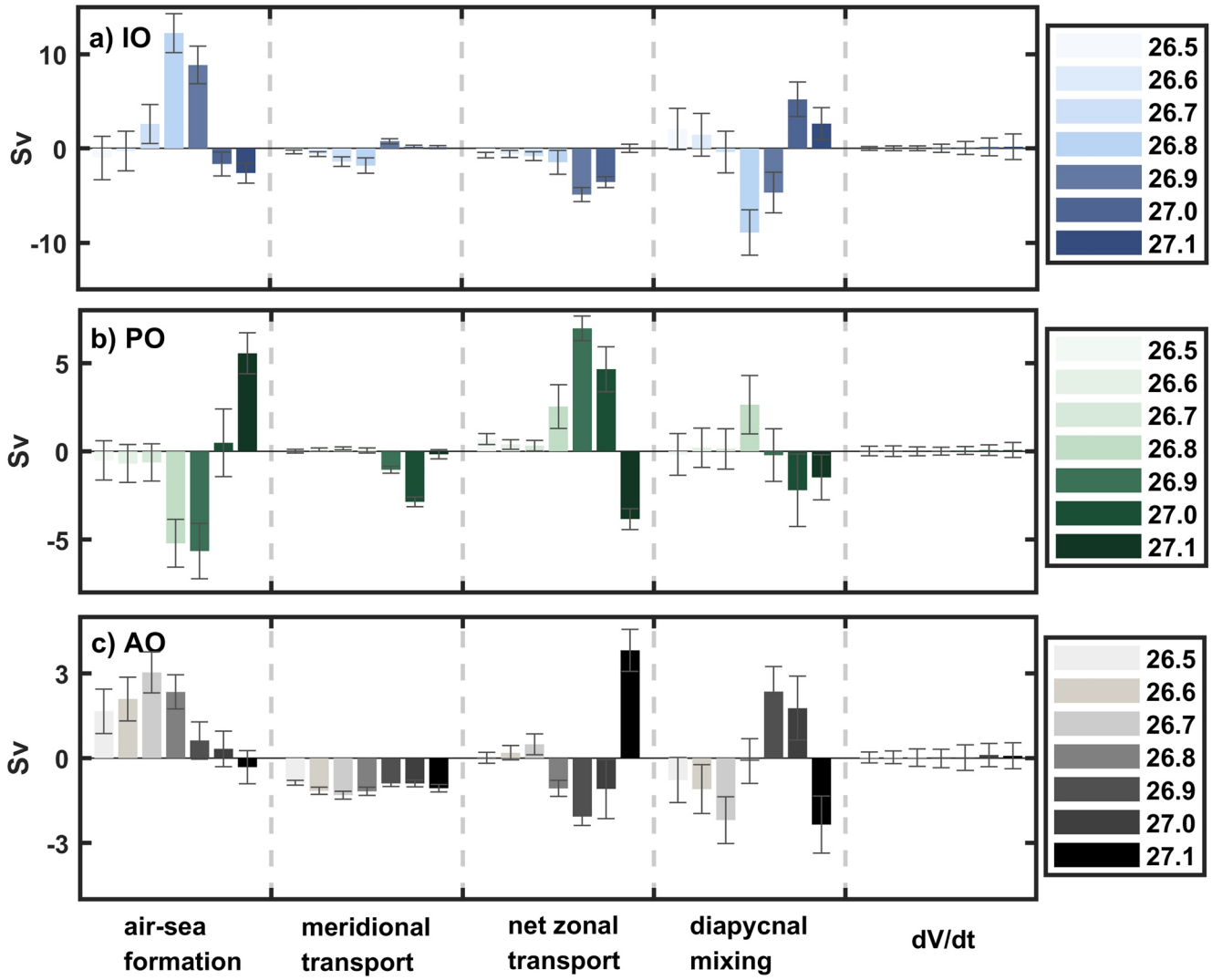

Figure 5. Climatological mean Subantarctic Mode Water volume budget terms for individual isopycnal layers in the (a) Indian Ocean, (b) Pacific Ocean, and (c) Atlantic Ocean. The climatological mean is obtained by averaging over the period of 1950–2017. The error bars denote the standard deviations of annual mean values during 1950–2017.

formation from air–sea buoyancy fluxes has also been found in previous studies (Cerovečki et al., 2013; Cerovečki & Mazloff, 2016; Sloyan & Rintoul, 2001). However, a further examination of individual isopycnal layers (Figure 5b) indicates that the air–sea buoyancy fluxes actually form SAMW in the denser layers (27.0–27.1 kg m^{-3}), but this formation is smaller than its destruction in the lighter layers (26.5–26.9 kg m^{-3}). The supply by zonal transport occurs mainly at 26.9 and 27.0 kg m^{-3}. Diapycnal mixing acts to form SAMW at 26.8 kg m^{-3} but destroys SAMW at 27.0 and 27.1 kg m^{-3}, and overall, it makes a trivial contribution to the SAMW volume budget in the PO.

In the AO (orange bars in Figure 4), SAMW is formed by air–sea buoyancy fluxes (8.9 ± 1.2 Sv), exported by meridional transport (7.4 ± 0.4 Sv), and destroyed by diapycnal mixing (1.1 ± 1.0 Sv). In more detail, Figure 5c shows that while both formations by air–sea buoyancy fluxes and export by meridional transport occur in all isopycnal layers, the overall minor contributions from zonal transport and diapycnal mixing to the SAMW volume budget are a result of cancellation in different isopycnal layers.

In summary, considering the entire SAMW density range, the air–sea buoyancy fluxes form SAMW in the IO and AO but destroy SAMW in the PO. However, by considering separately lighter and denser varieties of SAMW in the PO, it is evident that the air–sea buoyancy fluxes form SAMW in the denser density range

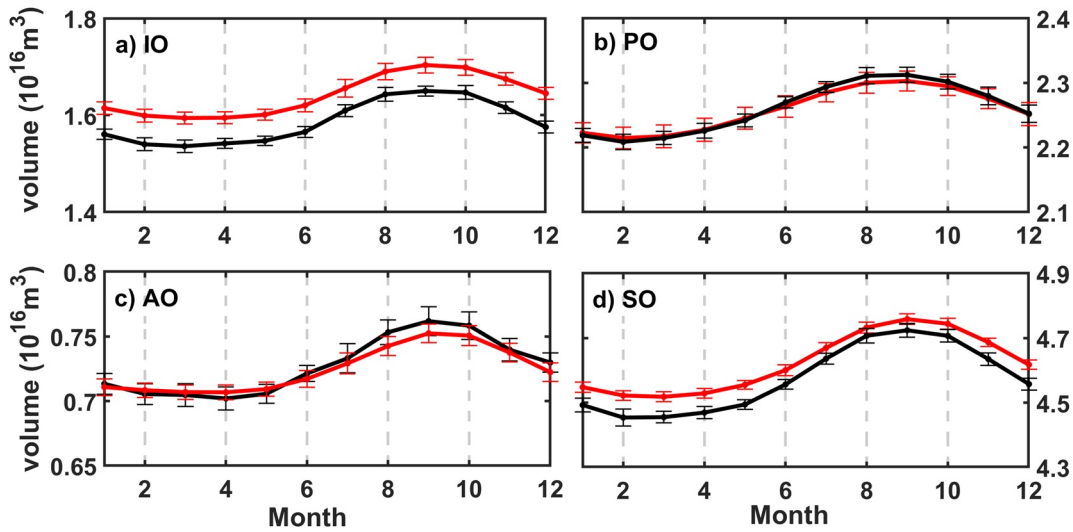

Figure 6. Annual cycle of the Subantarctic Mode Water volume from ocean general circulation model for the Earth (red lines) and Argo (black lines) in the (a) Indian Ocean, (b) Pacific Ocean, (c) Antlantic Ocean, and (d) Southern Ocean. The monthly climatology is obtained by averaging over the period of 2004–2017. The error bars denote standard deviations for each month during 2004–2017.

(27.0–27.1 kg m^{-3}) by destroying the lighter water (26.5–26.9 kg m^{-3}) and transforming it into denser water. Meridional advection transports SAMW to the subtropical regions in all three ocean sectors. The zonal transport exports SAMW from the IO and imports it to the PO. Diapycnal mixing acts to destroy SAMW in the IO. For the SO as a whole (gray bars in Figure 4), our estimation finds that the climatological mean SAMW volume is balanced between the following: formation by air–sea buoyancy fluxes (19.6 ± 2.7 Sv), removal by advective export northward across 30°S (14.2 ± 0.9 Sv), destruction by diapycnal mixing (3.1 ± 2.2 Sv), and net storage (2.3 ± 2.6 Sv).

3.2. Annual Cycle

The annual cycle of the SAMW volume in each ocean sector is shown in Figure 6. It is clear that the SAMW volume has a significant seasonal variation, with the maximum in September and the minimum in March in all of the ocean sectors. The volume increase or formation of SAMW from March to September is $1.2 \pm 0.1 \times 10^{15}$ m^3, $0.9 \pm 0.1 \times 10^{15}$ m^3, $0.5 \pm 0.1 \times 10^{15}$ m^3, and $2.6 \pm 0.2 \times 10^{15}$ m^3 in the IO, PO, AO, and entire SO, respectively. In comparison with the observations, Figure 6 also shows that the model captures the annual cycle of the SAMW volume well.

Figure 7 shows the annual cycle of the SAMW volume budget in each ocean sector. The rate of volume change is positive from April to September and negative from October to March for all ocean sectors, indicating that SAMW forms during the former period of time and is destroyed during the latter period of time. This also corresponds to the maximum volume of SAMW in September and the minimum volume of SAMW in March (Figure 6). In addition, for all three ocean sectors, the seasonal variation in the formation due to air–sea buoyancy fluxes appears to closely follow that of the volume change, suggesting that the SAMW volume change is primarily dominated by the formation of air–sea buoyancy fluxes in the annual cycle. This result is consistent with that of Cerovečki and Mazloff (2016), who found that on the seasonal time scale, the formation of SAMW is predominantly balanced by its volume storage. The results of this study also emphasize that wintertime surface buoyancy fluxes play a dominant role in forming SAMW (e.g., McCartney, 1977; Sloyan & Rintoul, 2001). Furthermore, while advection does not change much during the seasonal cycle, diapycnal mixing contributes to the seasonal variation in the SAMW volume, particularly during the winter season (Figure 7). This result is consistent with that of previous studies (Iudicone, Madec, Blanke, & Speich, 2008; Kwon, 2013; Marshall et al., 1999), in which the effect of diapycnal mixing is

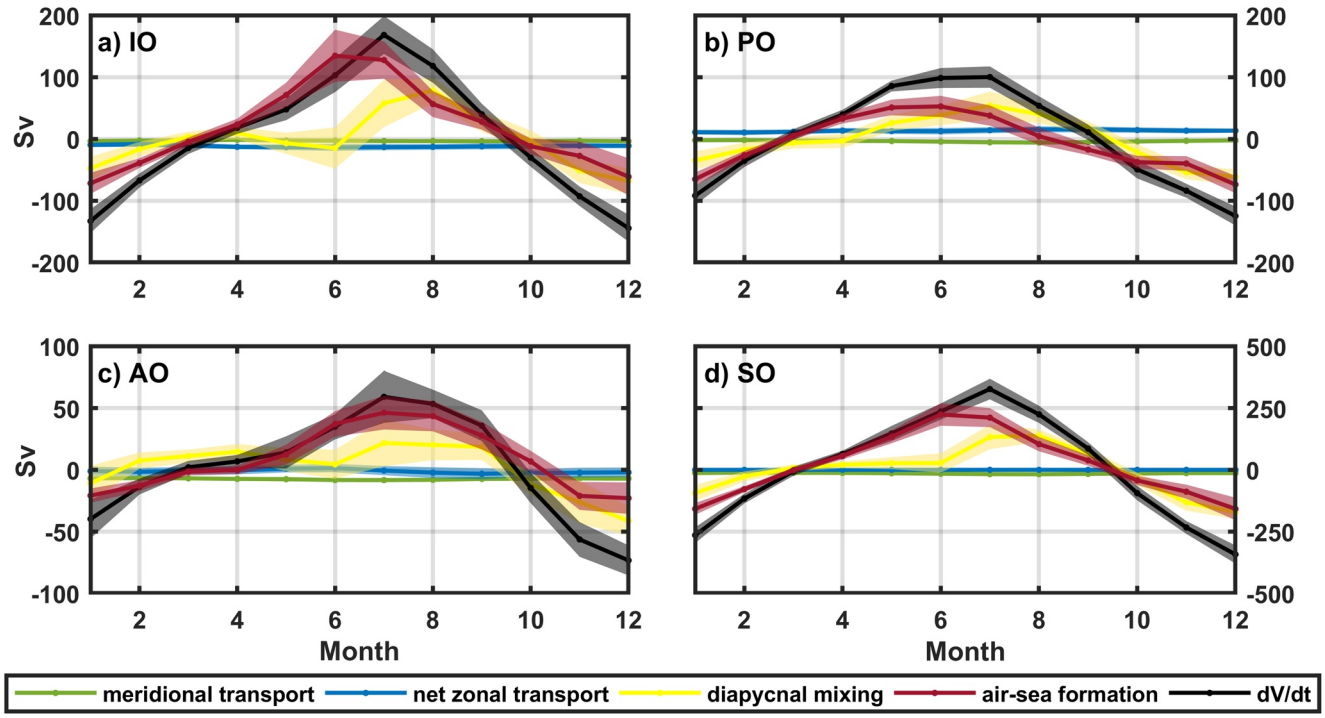

Figure 7. Annual cycle of the Subantarctic Mode Water volume budget from air–sea formation (red lines), meridional transport (green lines), net zonal transport (blue lines), diapycnal mixing (yellow lines), and storage rate (black lines) in the (a) Indian Ocean, (b) Pacific Ocean, (c) Atlantic Ocean, and (d) Southern Ocean. The monthly climatology is obtained by averaging over the period of 1950–2017. The color shading indicates the standard deviations during the 68 years of simulations.

the greatest during the winter when the convection process helps to deepen the mixed layer over the mode water formation regions.

4. Interannual Variability

Figure 8 shows the interannual variability of the SAMW volume budget terms. While meridional transport has minor changes, air–sea formation, net zonal transport, and diapycnal mixing all appear to have significant variations in all three ocean sectors. The storage rate oscillates around zero, suggesting that a dynamic balance is reached among the air–sea formation, diapycnal mixing, and advective transports. Further analysis reveals that the storage rate is closely correlated to the air–sea formation on the interannual time scale, with their correlation coefficients being 0.73, 0.71, and 0.55 in the IO (Figure 8a), PO (Figure 8b), and AO (Figure 8c) at the 99% confidence level, respectively. This suggests that the SAMW volume tends to be large in the year when more SAMW is formed by the air–sea buoyancy fluxes. The important role of air–sea buoyancy fluxes in the interannual variability in the SAMW formation is also suggested by previous studies (Naveira Garabato et al., 2009; Tamsitt et al., 2020). In addition, the interannual variability in the storage rate is also related to the net zonal transport in the AO and PO, with a correlation coefficient of 0.57 in the AO (Figure 8c) and 0.3 in the PO (Figure 8b) at the 99% confidence level.

Since the storage rate is closely related to the air–sea formation and net zonal transport on the interannual time scale, we next examine these three terms in individual isopycnal layers as well as their relationships. In the IO, the SAMW volume has more significant interannual variations in the 26.6–26.9 kg m^{-3} density layers (Figure 9a). In particular, the volume appeared to have opposite changes between 26.6–26.7 kg m^{-3} and 26.8–26.9 kg m^{-3}. This result is consistent with that of Hong et al. (2020), who suggested that the lighter (26.6–26.7 kg m^{-3}) and denser (26.8–26.9 kg m^{-3}) SAMW in the IO varied predominantly out of phase with each other during 2004–2018. The changes in the SAMW volume are clearly dominated by a air–sea formation (comparing Figures 9a with 9d), with net zonal transport having a minor contribution (comparing Figures 9a with 9g).

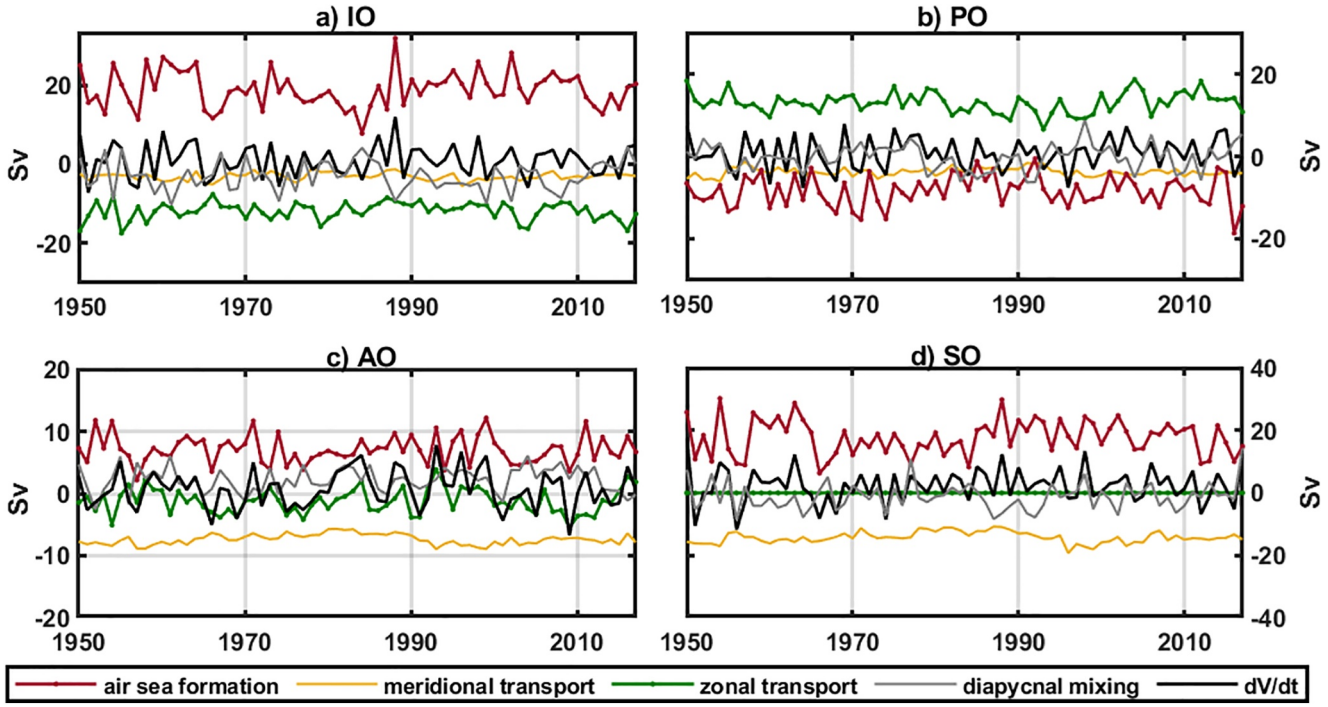

Figure 8. Interannual variability in the Subantarctic Mode Water volume budget terms in the (a) Indian Ocean, (b) Pacific Ocean, (c) Antlantic Ocean, and (d) Southern Ocean.

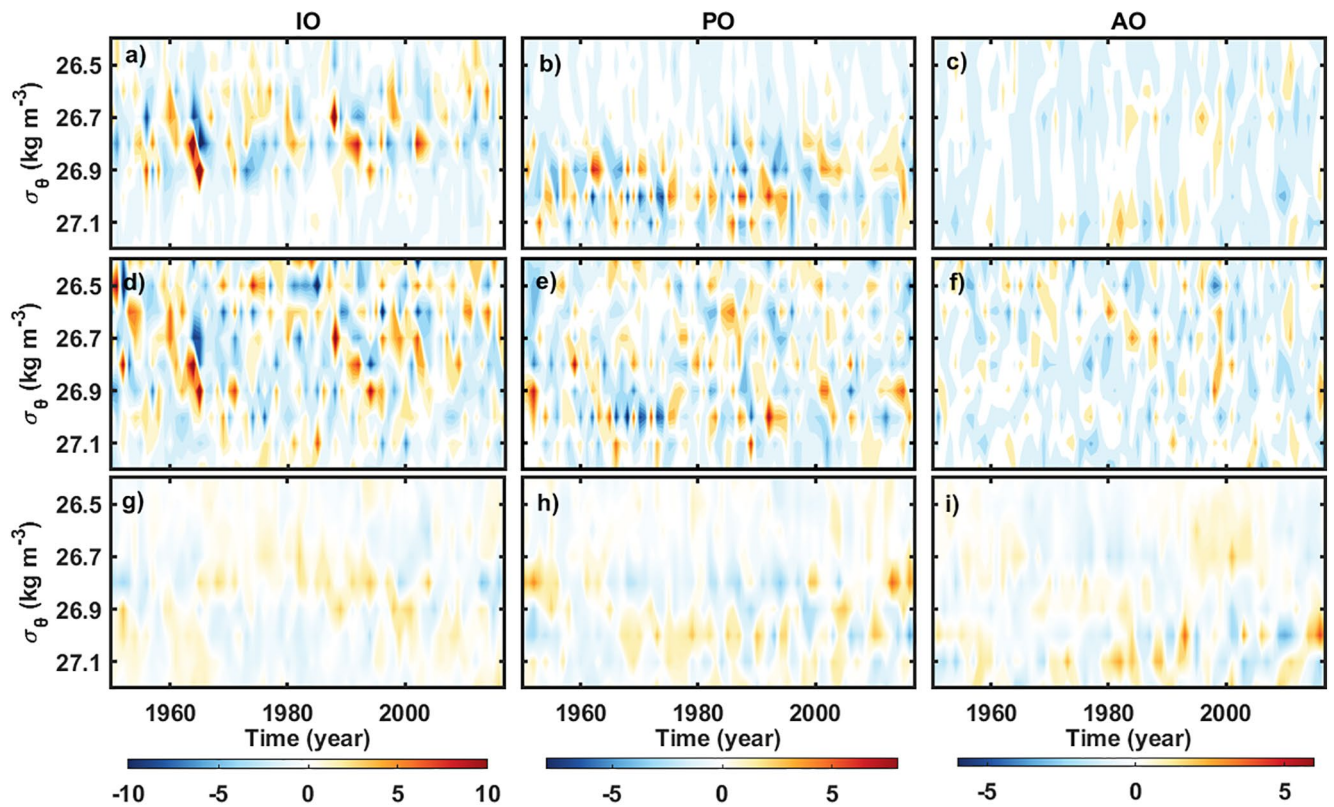

Figure 9. Time-density diagram of (a–c) storage rate; (d–f) anomalous air–sea formation; and (g–i) anomalous net zonal transport in the Indian Ocean (left), Pacific Ocean (middle), and Antlantic Ocean (right).

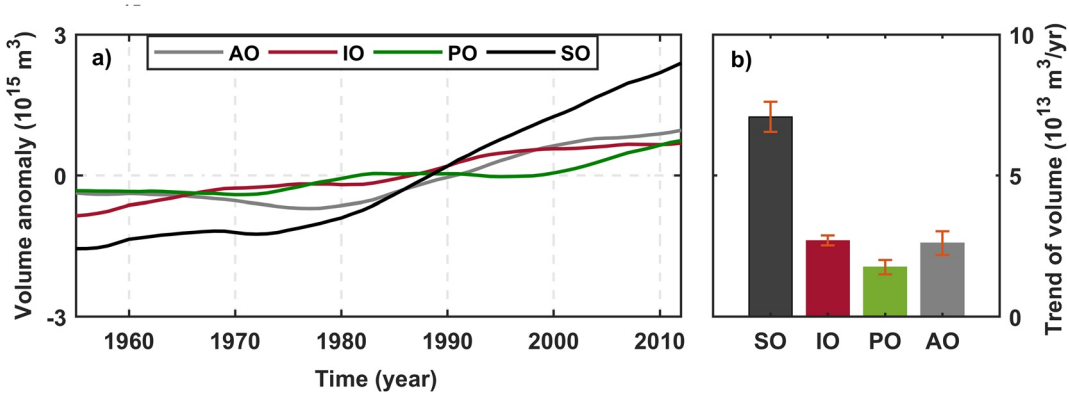

Figure 10. (a) 11-year running time series for anomalous Subantarctic Mode Water volumes and (b) their trends during 1950–2017. Linear trends are computed using the least squares linear fit and statistically tested with the Student's t test at the 95% confidence level (Leyba et al., 2019). The standard error in (b) is determined using the effective degree of freedom present in the regression residuals (Santer et al., 2000).

In the PO, large volume variations mainly occur in 26.8–27.1 kg m^{-3} density layers (Figure 9b), and similar to what happens in the IO, the volume changes are opposite between 26.9 kg m^{-3} and 27.0 kg m^{-3}. For example, during the 1990s (2000s), the SAMW volume tended to decrease (increase) by approximately 26.9 kg m^{-3} but increase (decrease) by approximately 27.0 kg m^{-3}. The opposite changes in the SAMW volume between different density layers in the IO and PO during the most recent decade are basically in agreement with previous studies (Cerovečki & Meijers, 2021; Hong et al., 2020; Meijers et al., 2019; Portela et al., 2020; Tamsitt et al., 2020). For example, Tamsitt et al. (2020) found a dipole structure of winter ocean heat loss in both the IO and PO, which directly affects SAMW formation in different density layers. Cerovečki and Meijers (2021) showed that in years with the preferential formation of denser varieties of SAMW in the IO and PO, the formation of lighter varieties of SAMW is anomalously weak, and this dipole mode is associated with the air–sea heat flux, which is in turn affected by the zonal and meridional winds.

A comparison of Figure 9b with Figures 9e and 9h suggests that while air–sea formation still plays an important role in modifying the SAMW volume, the net zonal transport appears to make a significant contribution during some years and in some density layers. In the AO, the volume variation is relatively small in individual isopycnal layers (Figure 9c), and its correlations with the air–sea formation and net zonal transport are not as clear as in the IO and PO.

In addition, the net zonal transport appears to compensate each other in denser layers between the IO and PO (Figures 9g and 9h) and in lighter layers between the AO and IO (Figures 9g and 9i). For example, in the 1980s, less SAMW in the 26.8 kg m^{-3} isopycnal layer was exported out of the IO and imported into the PO, while in the 2000s, less SAMW in the 26.6–26.7 kg m^{-3} isopycnal layers was exported out of the AO and imported into the IO.

5. Decadal Variability and Long-Term Change

In addition to the seasonal and interannual variations discussed above, the SAMW volume appears to have had an increasing trend during 1950–2017. As shown in Figure 10b, the SAMW volume in the SO increased at a rate of $7.0 \pm 0.5 \times 10^{13} m^3/yr$, in which the IO, AO, and PO contributed 38% ($2.7 \pm 0.2 \times 10^{13} m^3/yr$), 37% ($2.6 \pm 0.3 \times 10^{13} m^3/yr$), and 25% ($1.7 \pm 0.4 \times 10^{13} m^3/yr$), respectively. Overall (Figure 10a), the SAMW volume in the SO increased by $4.8 \times 10^{15} m^3/yr$ from 1950 to 2017, which is ~11% of the total volume of SAMW (see Table 1).

The above finding is in agreement with previous studies based on observational datasets (Gao et al., 2017; Häkkinen et al., 2016). For example, Gao et al. (2017) analyzed Argo data and found an increased volume of SAMW (26.5–27.1 kg m^{-3}) during 2005–2015. By using observations and reanalysis data, Häkkinen et al. (2016) speculated a volume increase in SAMW from 1957 to 2011 because of the nonuniform deepening of isopycnals in the SO. However, our finding is in contrast to that of Xu et al. (2021), who also analyzed

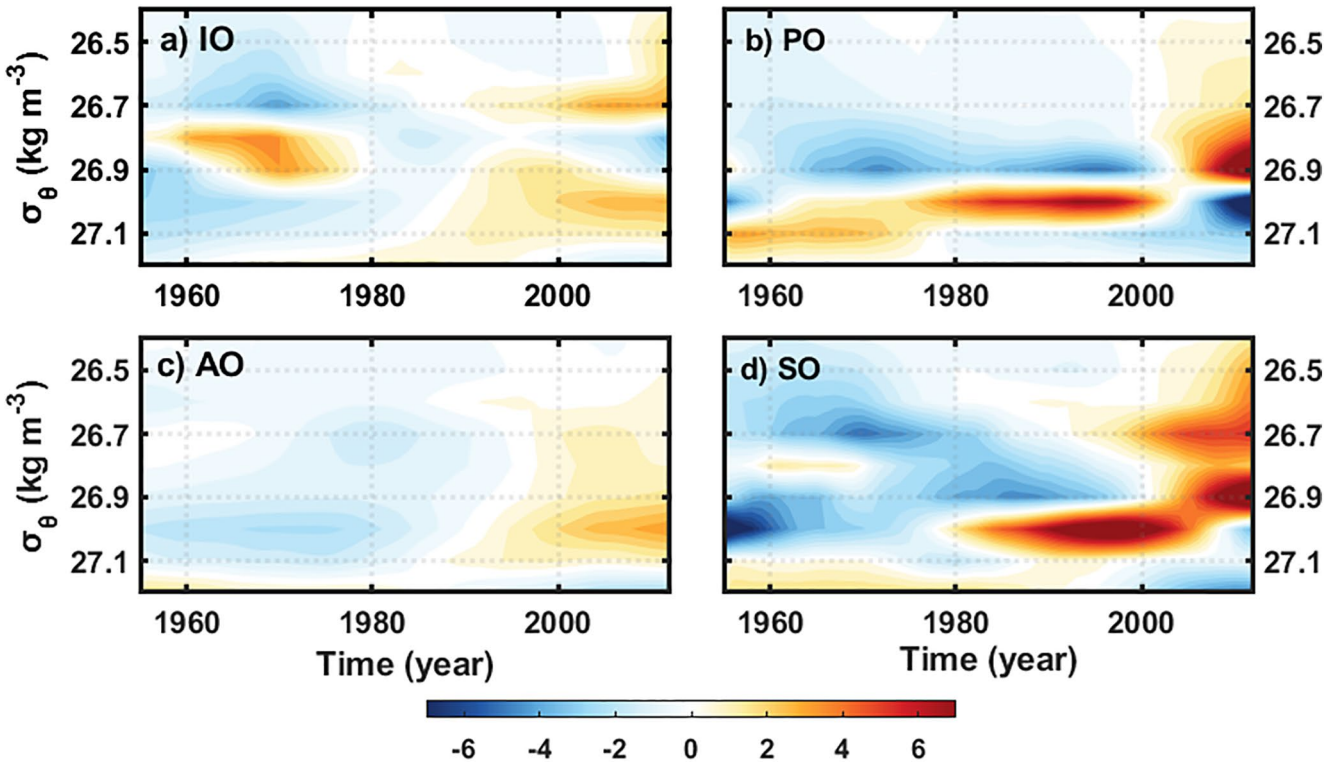

Figure 11. Time density of the 11-year running mean of the anomalous Subantarctic Mode Water volume (10^{14} m^3) in the (a) Indian Ocean, (b) Pacific Ocean, (c) Antlantic Ocean, and (d) Southern Ocean.

the Argo data and OFES output. While focusing on the SAMW property trends during the Argo period of 2004–2019, their study suggests that SAMW has become weaker, implying a decrease in volume, during the past several decades. This finding is because they identify SAMW as a layer with a low PV and a dynamic density range.

Figure 10a also shows that the long-term trends are superimposed on decadal variability. For example, the SAMW volume in the AO was small during the 1970s and 1980s but large during the 1990s and 2000s. In particular, the decadal changes in the SAMW volume in the IO and PO appear to compensate each other, with a correlation coefficient of −0.61 (at the 95% confidence level) after removing their long-term trends. This relationship, which is also evident in Figures 9g and 9h and discussed earlier, is due to low-frequency variations in the advective transport from the IO to the PO.

Figure 11 shows the SAMW volume changes in individual isopycnal layers. The most striking feature is that there are opposing volume changes with similar amplitudes in the upper and lower layers on a decadal time scale. In the IO (Figure 11a), a negative (positive) anomaly at 26.7 kg m^{-3} corresponds to a positive (negative) anomaly at 26.8 kg m^{-3} during the 1960s and 1970s (since early 2000). In the PO (Figure 11b), a negative (positive) anomaly at 26.9 kg m^{-3} corresponds to a positive (negative) anomaly at 27.0 kg m^{-3} during the 1980s and 1990s (since early 2000). Collectively (Figure 11d), SAMW in the SO appears to have an increase in volume, with a tendency to emerge gradually from denser layers to lighter layers. This is consistent with previous studies (Close et al., 2013; Portela et al., 2020). For example, Close et al. (2013) found that SAMW has experienced substantial lightening since the 1970s. Portela et al. (2020) found that there was a lightening of the upper waters in the Southern Hemisphere during the Argo era. The lightening of SAMW coincides with a warming trend in the upper ocean in observations (Desbruyères et al., 2017; Gao et al., 2017; Häkkinen et al., 2016; Kolodziejczyk et al., 2019).

This so-called two-layer density structure of SAMW in the IO and PO has been identified by Portela et al. (2020) with Argo observations, who found that during 2006–2015, the upper layer gains volume while the lower layer loses volume. During the past decade, a volume increase in the 26.8 and 26.9 kg m^{-3}

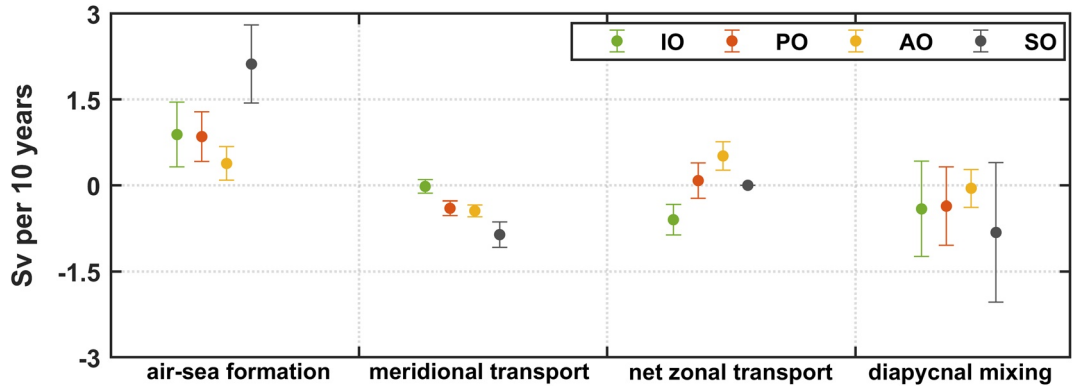

Figure 12. Linear trends of annual mean air–sea formation, meridional transport, net zonal transport, and diapycnal mixing during 1950–2017. Trends are statistically tested with the Student's t test at the 95% confidence level, and the standard error is determined using the effective degree of freedom present in the regression residuals.

isopycnal layers in the PO was also reported by Kolodziejczyk et al. (2019). Furthermore, our analysis also finds that the two-layer density structure of SAMW existed before the Argo era, but its changes were reversed, that is, the upper layer lost volume while the lower layer gained volume before the early 2000s in the PO (Figure 11b) and during the 1960s and 1970s in the IO (Figure 11a). In addition, this relationship also seemed to exist in the AO but in the denser layers, and the reversal occurred in the mid-1980s (Figure 11c).

To understand the processes that cause the long-term increase in the SAMW volume, we estimate the contributing terms in Equation 5 and their trends during 1950–2017, which are presented in Figure 12. It is clear that air–sea formation is significantly increased in all three ocean sectors, indicating its positive role in increasing the SAMW volume. In the PO and AO, meridional transport northward across 30°S is significantly enhanced and thus contributes negatively to the volume increase. The zonal transports out of the AO and into the IO are also significant, but they compensate each other, while there is no significant trend of diapycnal mixing in all three ocean sectors. Therefore, overall in the SO, the increased SAMW volume since the 1950s is mainly the result of an increase in the formation due to air–sea buoyancy fluxes. This result is basically in agreement with Karstensen and Quadfasel (2002), who analyzed NCEP/NCAR reanalysis data and found a consistent increase in the formation of thermocline water in the Southern Hemisphere oceans from 1950 to 1999. Furthermore, they suggested that this increase would lead to an increase in thermocline waters.

Next, we examine the transformation rates across 27.1 kg m^{-3} and 26.5 kg m^{-3} to reveal the reason for the increase in air–sea formation over the outcropping area between these two isopycnals during 1950–2017. Note that, as shown in Figure 13, the annual mean transformation rates are opposite across 26.5 kg $m^{-3}$and 27.1 kg m^{-3}. This is because, on an annual average, the ocean loses (gains) buoyancy over the outcropping area by approximately 26.5 (27.1) kg m^{-3}, leading to lighter (denser) water being transformed into the SAMW density range and thus a positive (negative) transformation rate. It is clear in Figure 13 that while the interannual and decadal variability in air–sea formation is partially dominated by the transformation rate across 26.5 kg m^{-3}, its increase during 1950–2017 is entirely attributable to a consistent decrease in the transformation rate across 27.1 kg m^{-3}, which is in turn due to an increase in oceanic buoyancy gain over the outcropping area at approximately 27.1 kg m^{-3}. Therefore, we conclude that the increased buoyancy gain by the ocean over the outcropping area of approximately 27.1 kg m^{-3} leads to more dense water being transformed into the SAMW density range and thus has increased the SAMW volume since the 1950s.

6. Summary and Discussions

The climatological mean, seasonal, interannual, and decadal variability, as well as the long-term change in the SAMW volume, are investigated based on the 0.1° OFES output from 1950 to 2017. The whole SO is divided into the IO, PO, and AO. The SAMW volume budget is analyzed in each individual ocean sector, and the relative contribution of each process to the volume budget is examined.

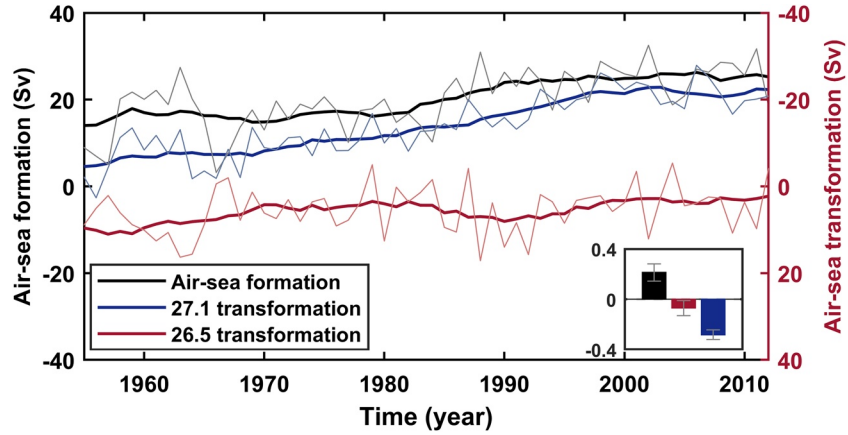

Figure 13. Variability in the annual mean air–sea formation rate of Subantarctic Mode Water in the Southern Ocean (thin black line; left axis) and annual mean transformation rate (positive indicates a transformation toward denser water) across 26.5 kg m^{-3} (thin red line; right axis) and 27.1 kg m^{-3} (thin blue line; right axis), with their trends shown in the inset. The thick lines are their 11-year running time series. Linear trends are computed using the least squares linear fit and statistically tested with the Student's t test at the 95% confidence level. The standard error in the inset is determined using the effective degree of freedom present in the regression residuals. Note that the *y*-axis on the right is reversed. The black line is the difference between the red line and blue line.

In the climatological mean, ~49% of the total SAMW volume in the SO is located in the PO, with the rest from the IO (~36%) and AO (~15%). Considering the entire SO, SAMW is formed by air–sea buoyancy fluxes, approximately 70% of which is exported northward to the subtropics, and the remainder is destroyed by diapycnal mixing. Specifically, SAMW in the IO is formed by air–sea buoyancy fluxes and removed by zonal advection into the PO, meridional transport across 30°S, and diapycnal mixing. In the PO, SAMW is supplied by zonal advection from the IO and removed by air–sea buoyancy fluxes and meridional transport across 30°S, with diapycnal mixing making minor contributions. In the AO, SAMW is formed by air–sea buoyancy fluxes and exported to the subtropics by meridional advection, with both zonal advection and diapycnal mixing having minor contributions.

Seasonally, the SAMW volume reaches the maximum in September and the minimum in March in all three ocean sectors. The seasonal cycle of the SAMW volume is dominated by air-sea buoyancy fluxes, that is, SAMW is formed during austral winter when the ocean loses buoyancy to the atmosphere.

On the interannual time scale, while meridional transport shows minor variability, air–sea formation, zonal transport, and diapycnal mixing appear to have significant variations in all three ocean sectors. In addition, in all three ocean sectors, the storage rate of the SAMW volume is closely correlated to the air-sea formation, that is, the storage rate tends to be large in years when more SAMW is formed by air-sea buoyancy fluxes. Furthermore, in the AO and PO, the storage rate is also related to the net zonal transport.

Decadal changes in the SAMW volume in the IO and PO feature a two-layer density structure, in which the volumes of the upper and lower layers vary predominantly out of phase with each other. In addition, SAMW in the SO had a significant increase in volume (~11%) during 1950–2017, which tended to emerge gradually from denser to lighter layers. The increase in the SAMW volume resulted from increased air-sea formation, which in turn arose from an increase in oceanic buoyancy gain over the outcropping area of approximately 27.1 kg m^{-3}. The increased buoyancy gain by the ocean over the outcropping area of approximately 27.1 kg m^{-3} leads to denser water being transformed into the SAMW density range and thus has increased the SAMW volume since the 1950s.

The diapycnal mixing represents the net effect of all mixing processes (e.g., eddy stirring, boundary layer dynamics, wave breaking, and wind mixing; Cerovečki et al., 2013; Nishikawa et al., 2013). However, water formation/destruction due to diapycnal mixing is difficult to calculate directly from model outputs and is often estimated as a residual of the other terms in the volume budget equation (e.g., Cerovečki et al., 2013; Downes et al., 2011; Marsh et al., 2000). Thus, the resulting diapycnal mixing is affected by the uncertainty

associated with the other terms. For example, an underestimation of air–sea formation could result in an overestimation of the formation due to diapycnal mixing. In addition, since we use the monthly OFES output, our analysis is not able to resolve shorter time-scale processes and thus their contribution to the formation/destruction by air–sea buoyancy fluxes (Cerovečki & Marshall, 2008; Garrett & Tandon, 1997), which could be instead attributed to diapycnal mixing. It would have therefore been preferable to evaluate the transformation due to diapycnal mixing by diagnosing each term in the volume budget (rather than estimating it as a residual), as suggested by Iudicone, Madec, and Mcdougall (2008), which has been applied in recent studies (Abernathey et al., 2016; Cerovečki & Mazloff, 2016).

Data Availability Statement

The 0.1° OFES output was provided by the Asia Pacific Data Research Center (http://apdrc.soest.hawaii.edu/dods/public_ofes/OfES/ncep_0.1_global_mmean). The Argo data were obtained from the Argo website (http://sio-argo.ucsd.edu/RG_Climatology.html).

Acknowledgments
The authors are grateful to the editor and three anonymous reviewers who provided extremely insightful and valuable feedback and suggestions. This work was supported by the National Natural Science Foundation of China (NSFC; 41976006 and 41676002) and the National Key Research and Development Program of China (2018YFA0605702).

References

Abernathey, R. P., Cerovečki, I., Holland, P. R., Newsom, E., Mazloff, M., & Talley, L. D. (2016). Water-mass transformation by sea ice in the upper branch of the Southern Ocean overturning. *Nature Geoscience*, *9*(8), 596–601. https://doi.org/10.1038/ngeo2749

Aoki, S., Hariyama, M., Mitsudera, H., Sasaki, H., & Sasai, Y. (2007). Formation regions of Subantarctic Mode Water detected by OFES and Argo profiling floats. *Geophysical Research Letters*, *34*(10), L10606. https://doi.org/10.1029/2007GL029828S

Aoki, S., Mizuta, G., Sasaki, H., Sasai, Y., Rintoul, S. R., & Bindoff, N. L. (2015). Atlantic–Pacific asymmetry of subsurface temperature change and frontal response of the Antarctic Circumpolar Current for the recent three decades. *Journal of Oceanography*, *71*(5), 623–636. https://doi.org/10.1007/s10872-015-0284-6

Cerovečki, I., & Giglio, D. (2016). North Pacific Subtropical Mode Water volume decrease in 2006–09 estimated from Argo observations: Influence of surface formation and basin-scale oceanic variability. *Journal of Climate*, *29*(6), 2177–2199. https://doi.org/10.1175/JCLI-D-15-0179.1

Cerovečki, I., & Marshall, J. (2008). Eddy modulation of air–sea interaction and convection. *Journal of Physical Oceanography*, *38*, 65–83. https://doi.org/10.1175/2007JPO3545.1

Cerovečki, I., & Mazloff, M. R. (2016). The spatiotemporal structure of diabatic processes governing the evolution of Subantarctic Mode Water in the Southern Ocean. *Journal of Physical Oceanography*, *46*(2), 683–710. https://doi.org/10.1175/JPO-D-14-0243.1

Cerovečki, I., & Meijers, A. (2021). Strong quasi-stationary wintertime atmospheric surface pressure anomalies drive a dipole pattern in the Subantarctic Mode Water formation. *Journal of Climate*, 1–44. https://doi.org/10.1175/JCLI-D-20-0593.1

Cerovečki, I., Meijers, A., Mazloff, M. R., Gille, S. T., Tamsitt, V. M., & Holland, P. R. (2019). The effects of enhanced sea ice export from the Ross Sea on recent cooling and freshening of the southeast Pacific. *Journal of Climate*, *32*, 2013–2035. https://doi.org/10.1175/JCLI-D-18-0205.1

Cerovečki, I., Talley, L. D., Mazloff, M. R., & Maze, G. (2013). Subantarctic Mode Water formation, destruction, and export in the eddy-permitting Southern Ocean state estimate. *Journal of Physical Oceanography*, *43*(7), 1485–1511. https://doi.org/10.1175/JPO-D-12-0121.1

Close, S. E., Naveira Garabato, A. C., Mcdonagh, E. L., King, B. A., Biuw, M., & Boehme, L. (2013). Control of mode and intermediate water mass properties in Drake Passage by the Amundsen Sea Low. *Journal of Climate*, *26*(14), 5102–5123. https://doi.org/10.1175/JCLI-D-12-00346.1

Deremble, B., & Dewar, W. K. (2013). Volume and potential vorticity budgets of Eighteen Degree Water. *Journal of Physical Oceanography*, *43*, 2309–2321. https://doi.org/10.1175/JPO-D-13-052.1

Desbruyères, D., McDonagh, E. L., King, B. A., & Thierry, V. (2017). Global and full-depth ocean temperature trends during the early twenty-first century from Argo and repeat hydrography. *Journal of Climate*, *30*(6), 1985–1997. https://doi.org/10.1175/JCLI-D-16-0396.1

Dong, S., Sprintall, J., Gille, S. T., & Talley, L. (2008). Southern Ocean mixed-layer depth from Argo float profiles. *Journal of Geophysical Research*, *113*(C6), C06013. https://doi.org/10.1029/2006JC004051

Downes, S. M., Gnanadesikan, A., Griffies, S. M., & Sarmiento, J. L. (2011). Water mass exchange in the Southern Ocean in coupled climate models. *Journal of Physical Oceanography*, *41*(9), 1756–1771. https://doi.org/10.1175/2011JPO4586.1

Gao, L., Rintoul, S. R., & Yu, W. (2017). Recent wind-driven change in Subantarctic Mode Water and its impact on ocean heat storage. *Nature Climate Change*, *8*(1), 58–63. https://doi.org/10.1038/s41558-017-0022-8

Garrett, C., & Tandon, A. (1997). The effects on water mass formation of surface mixed layer time-dependence and entrainment fluxes. *Deep Sea Research*, *44*(12), 1991–2006. https://doi.org/10.1016/S0967-0637(97)00055-1

Häkkinen, S., Rhines, P., & Worthen, D. L. (2016). Warming of the global ocean: Spatial structure and water-mass trends. *Journal of Climate*, *29*(13), 4949–4963. https://doi.org/10.1175/JCLI-D-15-0607.1

Hanawa, K., & Talley, L. D. (2001). Mode waters. In G. Siedler, J. Church, & J. Gould (Eds.), Ocean circulation and climate (Vol. 77, pp. 373–386). Academic. https://doi.org/10.1016/S0074-6142(01)80129-7

Hartin, C. A., Fine, R. A., Sloyan, B. M., Talley, L. D., Chereskin, T. K., & Happell, J. (2011). Formation rates of Subantarctic mode water and Antarctic intermediate water within the South Pacific. *Deep Sea Research Part I: Oceanographic Research Papers*, *58*(5), 524–534. https://doi.org/10.1016/j.dsr.2011.02.010

Hong, Y., Du, Y., Qu, T., Zhang, Y., & Cai, W. (2020). Variability of the Subantarctic Mode Water volume in the South Indian Ocean during 2004-2018. *Geophysical Research Letters*, *47*(10), e2020GL087830. https://doi.org/10.1029/2020GL087830

Iudicone, D., Madec, G., Blanke, B., & Speich, S. (2008). The role of Southern Ocean surface forcings and mixing in the global conveyor. *Journal of Physical Oceanography*, *38*(7), 1377–1400. https://doi.org/10.1175/2008JPO3519.1

Iudicone, D., Madec, G., & Mcdougall, T. J. (2008). Water-mass transformations in a neutral density framework and the key role of light penetration. *Journal of Physical Oceanography*, *38*(7), 1357–1376. https://doi.org/10.1175/2007JPO3464.1

Karstensen, J., & Quadfasel, D. (2002). Formation of southern hemisphere thermocline waters: Water mass conversion and subduction. *Journal of Physical Oceanography*, *32*(11), 3020–3038. https://doi.org/10.1175/1520-0485(2002)032<3020:foshtw>2.0.co;2

Kolodziejczyk, N., Llovel, W., & Portela, E. (2019). Interannual variability of upper ocean water masses as inferred from Argo array. *Journal of Geophysical Research: Oceans*, *124*, 6067–6085. https://doi.org/10.1029/2018JC014866

Kwon, E. Y. (2013). Temporal variability of transformation, formation, and subduction rates of upper Southern Ocean waters. *Journal of Geophysical Research: Oceans*, *118*(11), 6285–6302. https://doi.org/10.1002/2013JC008823

Leyba, I. M., Solman, S. A., & Saraceno, M. (2019). Trends in sea surface temperature and air–sea heat fluxes over the South Atlantic Ocean. *Climate Dynamics*, *53*, 4141–4153. https://doi.org/10.1007/s00382-019-04777-2

Li, Z., England, M. H., Groeskamp, S., Cerovečki, I., & Luo, Y. (2021). The Origin and Fate of Subantarctic Mode Water in the Southern Ocean. *Journal of Physical Oceanography*, *51*(9), 2951–2972. https://doi.org/10.1175/JPO-D-20-0174.1

Lu, Y., Talley, L. D., Cerovečki, I., Gille, S. T., Xie, S.-P., Mazloff, M. R., et al. (2020). *Southern Ocean deep mixed layers and ventilated mode waters: Eastward-propagating interannual climate variability* (pp. HE44C–2117). AGU Fall Meeting Abstract.

Marsh, R., Nurser, A. J. G., Megann, A. P., & New, A. L. (2000). Water mass transformation in the Southern Ocean of a global isopycnal coordinate GCM. *Journal of Physical Oceanography*, *30*(5), 1013–1045. https://doi.org/10.1175/1520-0485(2000)030<1013:wmtits>2.0.co;2

Marshall, J., Jamous, D., & Nilsson, J. (1999). Reconciling thermodynamic and dynamic methods of computation of water-mass transformation rates. *Deep Sea Research*, *46*(4), 545–572. https://doi.org/10.1016/S0967-0637(98)00082-X

McCartney, M. S. (1977). Subantarctic mode water. In M. V. Angel (Ed.), *A Voyage of Discovery: George Deacon 70th Anniversary volume* (pp. 103–119). Pergamon.

McCartney, M. S. (1982). The subtropical recirculation of mode waters. *Journal of Marine Research*, *40*, 427–464.

Meijers, A. J. S., Cerovečki, I., King, B. A., & Tamsitt, V. (2019). A see-saw in Pacific Subantarctic Mode Water formation driven by atmospheric modes. *Geophysical Research Letters*, *46*(22), 13152–13160. https://doi.org/10.1029/2019GL085280

Naveira Garabato, A. C., Jullion, L., Stevens, D. P., Heywood, K. J., & King, B. A. (2009). Variability of Subantarctic Mode Water and Antarctic Intermediate Water in the Drake Passage during the late-twentieth and early-twenty-first centuries. *Journal of Climate*, *22*(13), 3661–3688. https://doi.org/10.1175/2009JCLI2621.1

Nishikawa, S., Tsujino, H., Sakamoto, K., & Nakano, H. (2013). Diagnosis of water mass transformation and formation rates in a high-resolution GCM of the North Pacific. *Journal of Geophysical Research Oceans*, *118*(3), 1051–1069. https://doi.org/10.1029/2012JC008116

Nurser, A. J. G., Marsh, R., & Williams, R. G. (1999). Diagnosing water mass formation from air–sea fluxes and surface mixing. *Journal of Physical Oceanography*, *29*(7), 1468–1487. https://doi.org/10.1175/1520-0485(1999)029<1468:DWMFFA>2.0.CO;2

Orsi, A. H., Whitworth, T., III, & Nowlin, W. D., Jr (1995). On the meridional extent and fronts of the Antarctic Circumpolar Current. *Deep Sea Research*, *42*(5), 641–673. https://doi.org/10.1016/0967-0637(95)00021-W

Portela, E., Kolodziejczyk, N., Maes, C., & Thierry, V. (2020). Interior water-mass variability in the southern hemisphere oceans during the last decade. *Journal of Physical Oceanography*, *50*, 361–381. https://doi.org/10.1175/JPO-D-19-0128.s110.1175/jpo-d-19-0128.1

Qu, T., Gao, S., & Fine, R. A. (2020). Variability of the Sub-Antarctic Mode Water subduction rate during the Argo period. *Geophysical Research Letters*, *47*, e2020GL088248. https://doi.org/10.1029/2020GL088248

Rintoul, S. R., & England, M. H. (2002). Ekman transport dominates local air sea fluxes in driving variability of subantarctic mode water. *Journal of Physical Oceanography*, *32*(5), 1308–1321. https://doi.org/10.1175/1520-0485(2002)032<1308:etdlas>2.0.co;2

Roemmich, D., & Gilson, J. (2009). The 2004-2008 mean and annual cycle of temperature, salinity, and steric height in the global ocean from the Argo program. *Progress in Oceanography*, *82*(2), 81–100. https://doi.org/10.1016/j.pocean.2009.03.004

Sabine, C. L., Feely, R. A., Gruber, N., Key, R. M., Lee, K., Bullister, J. L., et al. (2004). The oceanic sink for anthropogenic CO_2. *Science*, *305*(5682), 367–371. https://doi.org/10.1126/science.1097403

Sallée, J.-B., Morrow, R., & Speer, K. (2008). Eddy heat diffusion and Subantarctic Mode Water formation. *Geophysical Research Letters*, *35*(5), L05607. https://doi.org/10.1029/2007GL032827

Sallée, J.-B., Speer, K. G., Rintoul, S. R., & Wijffels, S. (2010). Southern Ocean thermocline ventilation. *Journal of Physical Oceanography*, *40*(3), 509–529. https://doi.org/10.1175/2009JPO4291.1

Santer, B. D., Wigley, T. M. L., Boyle, J. S., Gaffen, D. J., Hnilo, J. J., Nychka, D., et al. (2000). Statistical significance of trends and trend differences in layer-average atmospheric temperature time series. *Journal of Geophysical Research*, *105*(D6), 7337–7356. https://doi.org/10.1029/1999JD901105

Sasaki, H., Nonaka, M., Masumoto, Y., Sasai, Y., Uehara, H., & Sakuma, H. (2008). An eddy-resolving hindcast simulation of the quasiglobal ocean from 1950 to 2003 on the Earth simulator. In *High resolution numerical modelling of the atmosphere and ocean* (pp. 157–185): Springer New York. https://doi.org/10.1007/978-0-387-49791-4_10

Sloyan, B. M., & Rintoul, S. R. (2001). Circulation, renewal, and modification of Antarctic Mode and Intermediate water. *Journal of Physical Oceanography*, *31*(4), 1005–1030. https://doi.org/10.1175/1520-0485(2001)0312.0.CO;2

Tamsitt, V., Cerovečki, I., Josey, S. A., Gille, S. T., & Schulz, E. (2020). Mooring observations of air–sea heat fluxes in two Subantarctic Mode Water formation regions. *Journal of Climate*, *33*(7), 2757–2777. https://doi.org/10.1357/10.1175/JCLI-D-19-0653.1

Walin, G. (1982). On the relation between sea-surface heat flow and thermal circulation in the ocean. *Tellus*, *34*(2), 187–195. https://doi.org/10.3402/tellusa.v34i2.10801

Xu, L., Ding, Y., & Xie, S.-P. (2021). Buoyancy and wind driven changes in Subantarctic Mode Water during 2004-2019. *Geophysical Research Letters*, *48*(8), e2021GL092511. https://doi.org/10.1029/2021GL092511